Branched DNA That Forms a Solid at 95 °C**

*Arunoday Singh, Mariyan Tolev, Martin Meng, Konstantin Klenin, Oliver Plietzsch, Christine I. Schilling, Thierry Muller, Martin Nieger, Stefan Bräse, Wolfgang Wenzel, and Clemens Richert**

Control over the structure of materials may be achieved by using predictable interactions, such as base pairing. Base pairing between DNA strands is emerging as one of the most versatile design principles of nanoconstruction.[1] A range of hybridization[2] and folding motifs[3] of linear and circular DNA have been reported. The flexibility of the design has been further expanded by linking oligonucleotides to synthetic branching elements or "cores".[4,5] The resulting construct can have properties not found in natural DNA. This includes DNA coated gold nanoparticles[6] that assemble into three dimensional aggregates, the melting transitions of which are exceptionally sharp.[7] Nanoparticle size and linker structure affect the association behavior,[8] and crystallization may be induced in favorable cases.[9]

For DNA hybrids with organic cores, the effect of linking the DNA to a branching element can be more dramatic still. Four arm hybrid **1** (Scheme 1) with its tetrahedral core was recently shown to assemble into a macroscopic material, even though its oligonucleotide arms are just dimers.[10] The assembly process is sequence specific, as demonstrated by mismatch controls, but the UV melting transitions are broad, not sharp as in the case of gold nanoparticles. Shortly after the publication of the unusually stable assemblies of **1**, the first designed DNA crystals were reported.[11] The fact that the association of the rigid triangle motifs that serve as rigid "cores" in these crystals is also driven by no more than dimer "sticky ends" again suggests that the rules for 3D construction of periodic assemblies are quite different from those of linear DNA.[12]

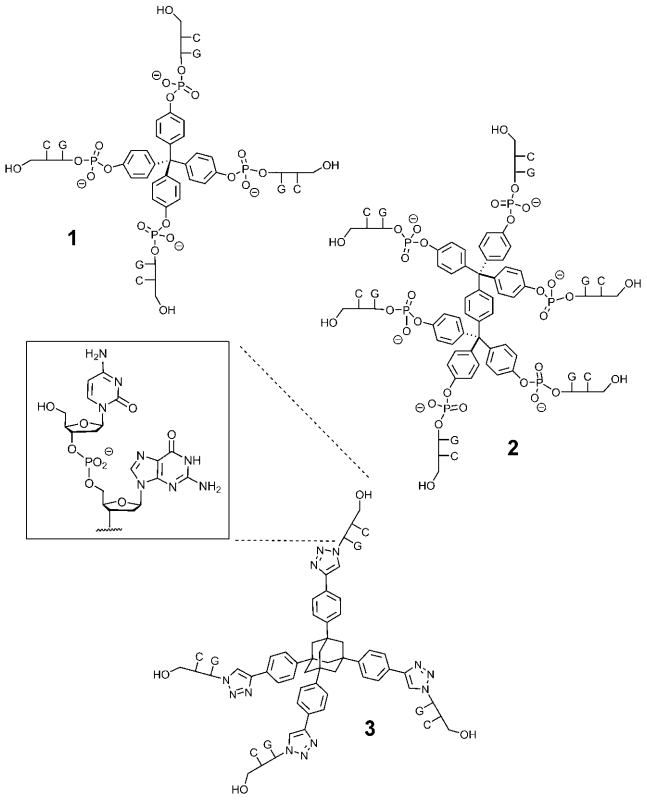

Scheme 1. Structures of the DNA hybrids employed: $(CG)_4$TPM (**1**), $(CG)_6$HPX (**2**), and $(CG)_4$TTPA (**3**). Abbreviations of cores are derived from those of the corresponding alcohols: TPM tetrakis(hydroxyphenyl)methane, HPX hexakis(hydroxyphenyl) *p* xylene, TTPA tetrakis(triazoylphenyl)adamantane.

We have modeled the assembly processes of hybrids by using an effective coarse grained model to better understand the effect of rigidity and core geometry on assembly. The theoretical results motivated the synthesis of new hybrids with greater propensity to assemble into three dimensional structures. Herein, we report two such hybrids, namely **2** with six DNA arms and pseudo octahedral core, and **3**, which forms a material from micromolar aqueous solution at 95 °C.

We performed Brownian dynamics simulations with geometric forms that hybridize via the ends of their arms as models for DNA hybrids. These uncharged, coarse grained models can reflect some key properties, such as size, coordination, and energy of bond formation as a function of bond angle and distance. To observe the assembly processes, the simulations had to be performed at high concentration (3 mM), and environmental effects (such as salt concentration,

[*] A. Singh, M. Tolev, Prof. C. Richert
Institut für Organische Chemie, Universität Stuttgart
70569 Stuttgart (Germany)
Fax: (+49) 711 685 64321
E mail: lehrstuhl 2@oc.uni stuttgart.de

M. Meng, O. Plietzsch, C. I. Schilling, Dr. T. Muller, Prof. S. Bräse
Institute of Organic Chemistry and Center for Functional Nano structures (CFN), Karlsruhe Institute of Technology (KIT)
76131 Karlsruhe (Germany)

Dr. M. Nieger
Laboratory of Inorganic Chemistry, Department of Chemistry
University of Helsinki, 00014 Helsinki (Finland)

Dr. K. Klenin, Priv. Doz. Dr. W. Wenzel
Institute for Nanotechnology
Karlsruhe Institute of Technology (KIT)
76021 Karlsruhe (Germany)

[**] This work was supported by CFN (project no. C5.01 03). We thank

electrostatic screening), required for quantitative prediction of the assembly temperature, cannot be adequately described. Simulations at half the concentration show a weak dependence of the assembly temperature on concentration, with a T_m depression of 4 8 °C.

Figure 1 a shows typical results of a tempering protocol. Hybrids with tetrahedral cores and flexible linkers were found to have a large propensity to form both five and six membered rings, thus leading to an arrangement without long range order (red structure in Figure 1 a; see the Supporting Information for definition of order parameter). The broad distribution of local bonding arrangements may explain why broad melting transitions are observed for **1**.[10] However, for stiffer hybrids (that is, small angular range for hybridization) we observed mostly six membered rings that coalesce into extended crystalline structures reminiscent of the two phases of ice in their local arrangement (blue structure in Figure 1 a). This indicates a significantly stronger propensity for the emergence of long range order for the rigid system, even though the bond energy per particle in the final structure is very similar to that of the more flexible system.

We then modeled the assembly of octahedrally coordinated hybrids, which were expected not to suffer from the problem of multiphase crystallites. Compared to the tetrahedral cores we found an increased tendency to form ordered structures with a near perfect coordination throughout the entire crystallites (Figure 1 a, green structure). This led to the search for a core with pseudo octahedral structure but no increase in flexibility over **1**.

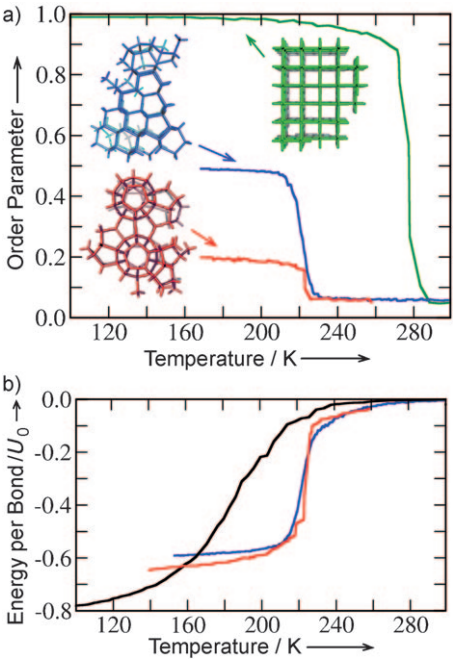

Figure 1. Modeling assembly processes. a) Order, but not energy, as a function of temperature for simulated adiabatic cooling of simplified models of hybrids with flexible tetrahedral (red), rigid tetrahedral (blue), or octahedral structure (green). b) Energy per bond (in units of artificial duplex strength) for tetrahedral hybrids with one active DNA arm (black, reference system) or four active arms and rigid (blue) or flexible (red) core DNA linkage. Models used are without the charge of actual DNA or its counterions.

Hybrid **2** was assembled starting from dimethyl terephthalate (**4**) via 1,4 phenylenebis[bis(4′ methoxyphenyl)methanol] (**5**) and HPX (**6**, hexakis(*p* hydroxyphenyl) *p* xylene;[13] see the Supporting Information). A crystal structure of **6** showed the expected pseudo octahedral geometry (Figure 2 a). The molecules are linked by intermolecular OH–O hydrogen bonds forming a two dimensional network of channels parallel to the crystallographic *a* and *b* axes with 53.1 % porosity, filled by five benzene guest molecules per unit cell and formula unit (Figure 2 b).

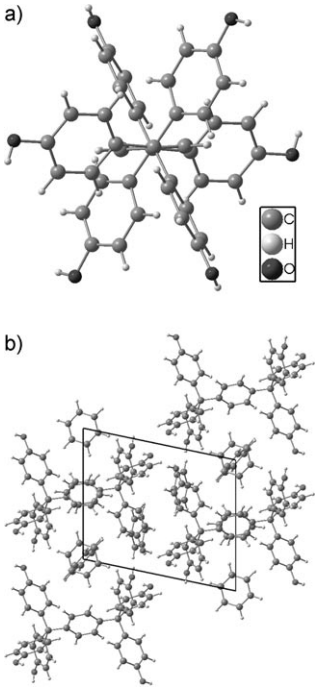

Figure 2. a) Molecular structure of **6** viewed along the xylene axis. b) Crystal packing with solvent benzene as guest. See the Supporting Information for further details.

Based on **6**, solid phase synthesis on controlled pore glass with a combination of 5′ and 3′ phosphoramidites and an on support phosphitylation step gave **2** in 5 % overall yield, after purification under denaturing conditions. Adamantane hybrid **3** was prepared next, using a solution phase synthesis that involved a cycloaddition and phosphoramidite coupling to elaborate the DNA arms[14] (see Scheme S3 in the Supporting Information). The strong tendency of this hybrid to self assemble required unconventional steps. A phosphoramidite coupling at 40 °C was followed by treatment with a mixture of oxidizing agents and detritylation with aqueous acid. Final deprotection with a mixture of ammonia and methylamine, and thorough washing of the basic solution, gave a crude product that was > 85 % pure (see Figure S4 in the Supporting Information). For HPLC, **3** was dissolved at 80 °C with 10 % CH_3CN and chromatographed with 10 mM buffer in the presence of organic solvent at 55 °C.

Figure 3 shows absorbance profiles of **1** **3** at 10 μM hybrid concentration, measured at 260 nm. Assays started under denaturing conditions (10 mM NaOH, 95 °C), followed by

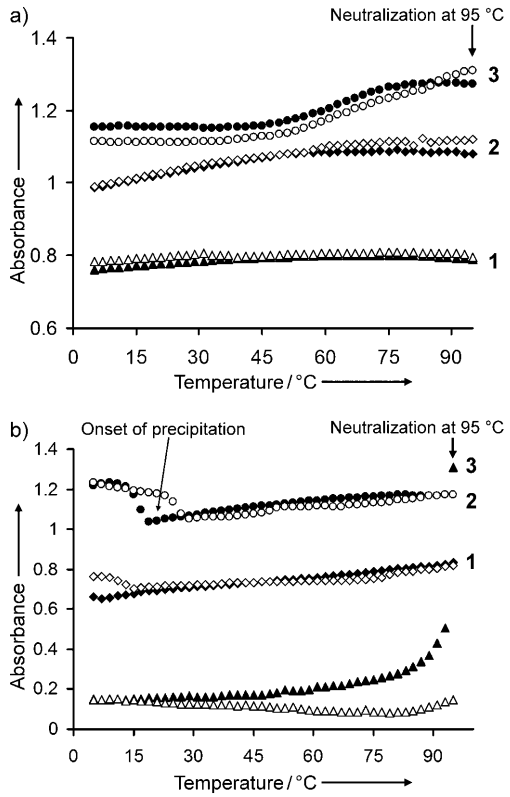

Figure 3. UV monitored thermal association and melting profiles (heating: open symbols, cooling: filled symbols) of 10 μM **1** **3** in a) 10 mM phosphate buffer, 1.5 mM NaOAc, or b) plus 150 mM NaCl and 100 mM $MgCl_2$. Increases in absorbance in the cold are caused by scattering on particles, while the sharp decrease in absorbance for **3** in the heat is a result of precipitation.

neutralization at 95 °C. At the hybrid concentration chosen and minimal salt concentration, **1** showed no transition, whereas both **2** and **3** gave association and melting curves with little hysteresis. Additional precipitation/melting curves acquired under other buffer conditions are presented in the Supporting Information.

After addition of NaCl and $MgCl_2$ and cooling, all hybrids showed macroscopic signs of assembly (Figure 4). The onset of particle formation depended strongly on structure (Table 1). Without magnesium, only **3** assembled visibly. After addition of divalent cations, six arm hybrid **2** started to form particles below 25 °C and flexible four arm hybrid **1** below 10 °C. For rigid hybrid **3** the propensity to assemble is most dramatic. This hybrid starts precipitating even at 95 °C, as evidenced by a sharp decrease in absorbance and settling of the material. The assemblies melted slowly during subsequent heating, as expected for solids (hysteresis between heating and cooling curves). The material formed by **3** did not fully redissolve upon reheating to 95 °C.

Linear DNA does not precipitate under our buffer conditions (see Figure S16 in the Supporting Information).

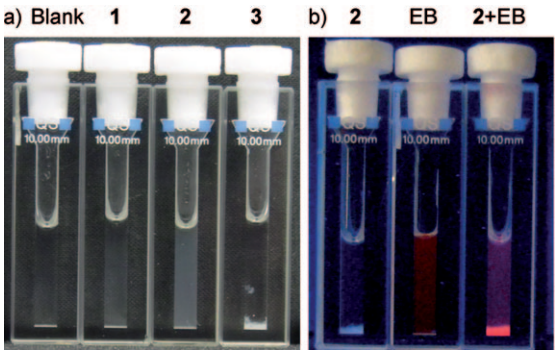

Figure 4. Photographs of cuvettes containing: a) samples of hybrids **1** **3** (10 μM), 150 mM NaCl, and 100 mM $MgCl_2$ at 20 °C under ambient light (**1** shows slight turbidity, both **2** and **3** show precipitation), and b) samples of **2** (38 μM), ethidium bromide (EB, 120 μM), and the precipitate of **2** soaked in EB (**2** + EB) under a hand held UV lamp (254 nm + 366 nm).

Table 1: UV melting points [°C] of assemblies formed by branched DNA hybrids at 10 μM concentration.

Compound	Buffer[a]	+ Na^{+}[b]	+ Mg^{2+}[c]
$(CG)_4$TPM (**1**)	n.t.[d]	14 ± 0.8	solid[e]
$(CG)_6$HPX (**2**)	18.7 ± 0.9	25.1 ± 1.3	solid[f]
$(CG)_4$TTPA (**3**)	61.5 ± 0.7	solid[g]	solid[g]

[a] 10 mM phosphate, 1.5 mM NaOAc, pH 7. [b] + 150 mM NaCl. [c] + 100 mM $MgCl_2$. [d] No cooperative transition. [e] Turbidity at ≤ 10 °C. [f] Turbidity at ≤ 25 °C. [g] Precipitation at ≤ 95 °C.

Control experiments with hybrids featuring non self complementary DNA arms, namely $(TC)_6$HPX and $(CC)_4$TTPA, demonstrated that the association is sequence specific, as predicted by the Watson Crick base pairing rules (see Figures S12 S15 in the Supporting Information). Similar controls for **1** were reported previously, together with a series of hybrids with longer DNA arms.[10] Analysis of precipitates harvested after 15 h at 4 °C by UV spectroscopy and MALDI TOF mass spectrometry confirmed that the precipitates contain intact hybrids (see Figures S18 S20 in the Supporting Information). Staining with duplex specific intercalator YOYO 1 indicates the formation of base pairs, and electron micrographs of particles show the formation of regularly shaped nanocrystals in precipitates (see Figures S17, S23, and S24 in the Supporting Information). For **3**, sufficient material was available to perform exploratory elemental analyses of precipitates. The CHN content is in agreement with approximately 40 % water and 24 equivalents of salt in the assemblies (see the Supporting Information).

Soaking preformed precipitates of pseudo octahedral hybrid **2** with intercalators for 15 h at 4 °C led to the uptake of approximately one equivalent of ethidium bromide per predicted CG:GC duplex and approximately 0.7 equivalents of methylene blue per predicted duplex (Figure 4b and the Supporting Information). This suggests that 1) a large proportion of the DNA arms engages in duplex formation, and 2) sufficient porosity exists for the intercalators to enter the material. Both properties are in agreement with the predicted

structure of **2** (green line, Figure 1 a). Larger crystallites than those shown in Figures S23 and S24 in the Supporting Information are required to confirm the structure of the solids by X ray crystallography. So far, we have been unable to grow such crystals.

To rationalize the ability of hybrids to assemble with just dimer DNA arms, we performed additional simulations. When three arms of a tetrahedral model system were deactivated to simulate duplex formation without multivalency, a much lower assembly temperature was found (black line, Figure 1 b). So, the increase in melting temperature when proceeding from conventional DNA dimers to **1** and then **2** found in calculations is in qualitative agreement with our experimental data. The additional massive increase in assembly temperature for **3** over **1** appears to be largely the result of electrostatics, as **3** has only four negative charges whereas **1** and **2** have eight and twelve, respectively.

Our results show how core structure and salt content affect the assembly process of branched DNA hybrids. By using CG "zippers" and organic cores, new materials are generated in a simple manner. The discovery of compounds such as **3** shows that many factors, including 1) increased rigidity, 2) reduced charge, 3) optimal fraction of organic, non DNA matter, and 4) appropriate counterions, must come together to achieve hybridization, and indeed solidification at temperatures where linear DNA remains fully dissociated. Growing macroscopic crystals and learning the rules for embedding functional molecules[15] or substrates in the cavities of hybrid assemblies are the next steps in the development of hybrid based functional materials.

In conclusion, we have shown the dramatic effect of multivalency and a rigid, uncharged linker on the association of branched DNA in dilute aqueous solution. Two base pairs per DNA arm suffice to induce formation of a new material at 95 °C. To the best of our knowledge, the hybridization properties of **3** are unprecedented for intermolecular duplex formation in the field of nucleic acid chemistry.[16]

Experimental Section

Modeling: A system consisting of 100 particles in the gas phase was subjected to Brownian dynamics simulated annealing and the final structures were analyzed. Particles interacted through four or six "arms", each of which represented a DNA linker attached to the core (corresponding to tetrahedral and octahedral symmetry, respectively). Two arms belonging to different particles interacted by an effective distance and angle dependent potential (see the Supporting Information). An order parameter was introduced by associating a straight (undirected) line in space with each arm. In a highly ordered or periodic system the orientations of these lines are strongly correlated and fall into a small number of large clusters, otherwise there are many different clusters of lines with different orientations. We characterized the degree of order at any point in the simulation by computing the fraction of particles contributing to the largest cluster of lines in the system (see the Supporting Information).

UV melting analysis: Lyophilized hybrid samples were taken up in NaOH solution (100 μL, 10 mM) and heated to 95 °C for full denaturation, followed by neutralization with acetic acid (100 μL, 10 mM) at 95 °C and addition of buffer (10 mM triethylammonium acetate or 10 mM phosphate buffer) to establish conditions for base pairing. For samples "with salt", stock solutions giving 150 mM NaCl and 100 mM $MgCl_2$ were added at 95 °C, and melting curves were measured with cooling or heating rates of 0.5 °C min^{-1} in a spectrometer with detection at 260 nm.

Crystal structure: CCDC 785245 (**6**) contains the supplementary crystallographic data for this paper. These data can be obtained free of charge from The Cambridge Crystallographic Data Centre via www.ccdc.cam.ac.uk/data request/cif. See also the Supporting Information.

Keywords: DNA · molecular modeling · nanostructures · oligonucleotides

[1] N. C. Seeman, *Nature* **2003**, *421*, 427 431.
[2] Selected references: a) J. T. Fu, Y. C. Tse Dinh, N. C. Seeman, *J. Mol. Biol.* **1994**, *236*, 91 105; b) Z. Shen, H. Yan, T. Wang, N. C. Seeman, *J. Am. Chem. Soc.* **2004**, *126*, 1666 1674; c) R. P. Goodman, I. A. T. Schaap, C. F. Tardin, C. M. Erben, R. M. Berry, C. F. Schmidt, A. J. Turberfield, *Science* **2005**, *310*, 1661 1665; d) J. Zimmermann, M. P. J. Cebulla, S. Monninghoff, G. von Kiedrowski, *Angew. Chem.* **2008**, *120*, 3682 3686; *Angew. Chem. Int. Ed.* **2008**, *47*, 3626 3630.
[3] Selected references: a) P. W. K. Rothemund, *Nature* **2006**, *440*, 297 302; b) H. Gu, J. Chao, S. J. Xiao, N. C. Seeman, *Nat. Nanotechnol.* **2009**, *4*, 245 248; c) S. M. Douglas, H. Dietz, T. Liedl, B. Högberg, F. Graf, W. M. Shih, *Nature* **2009**, *459*, 414 418.
[4] a) F. A. Aldaye, A. L. Palmer, H. F. Sleiman, *Science* **2008**, *321*, 1795 1799; b) U. Feldkamp, C. M. Niemeyer, *Angew. Chem.* **2006**, *118*, 1888 1910; *Angew. Chem. Int. Ed.* **2006**, *45*, 1856 1876; c) K. V. Gothelf, T. H. LaBean, *Org. Biomol. Chem.* **2005**, *3*, 4023 4037.
[5] Selected references: a) L. H. Eckardt, K. Naumann, W. M. Pankau, M. Rein, M. Schweitzer, N. Windhab, G. von Kiedrowski, *Nature* **2002**, *420*, 286; b) K. M. Stewart, J. Rojo, L. W. McLaughlin, *Chem. Commun.* **2003**, 2934 2935; c) K. M. Stewart, L. W. McLaughlin, *J. Am. Chem. Soc.* **2004**, *126*, 2050 2057; d) K. M. Stewart, J. Rojo, L. W. McLaughlin, *Angew. Chem.* **2004**, *116*, 5932 5935; *Angew. Chem. Int. Ed.* **2004**, *43*, 5808 5811; e) F. A. Aldaye, H. F. Sleiman, *Angew. Chem.* **2006**, *118*, 2262 2267; *Angew. Chem. Int. Ed.* **2006**, *45*, 2204 2209.
[6] a) C. A. Mirkin, R. L. Letsinger, R. C. Mucic, J. J. Storhoff, *Nature* **1996**, *382*, 607 609; b) A. P. Alivisatos, K. P. Johnsson, X. Peng, T. E. Wilson, C. J. Loweth, M. P. Bruchez, Jr., P. G. Schultz, *Nature* **1996**, *382*, 609 611; c) P. Hazarika, B. Ceyhan, C. M. Niemeyer, *Angew. Chem.* **2004**, *116*, 6631 6633; *Angew. Chem. Int. Ed.* **2004**, *43*, 6469 6471.
[7] T. A. Tanton, C. A. Mirkin, R. L. Letsinger, *Science* **2000**, *289*, 1757 1760.
[8] a) R. Jin, G. Wu, Z. Li, C. A. Mirkin, G. C. Schatz, *J. Am. Chem. Soc.* **2003**, *125*, 1643 1654; b) R. J. Macfarlane, M. R. Jone, A. J. Senesi, K. L. Young, B. Lee, J. Wu, C. A. Mirkin, *Angew. Chem.* **2010**, *122*, 4693 4696; *Angew. Chem. Int. Ed.* **2010**, *49*, 4589 4592.
[9] a) D. Nykypanchuk, M. M. Maye, D. van der Lelie, O. Gang, *Nature* **2008**, *451*, 549 552; b) S. Y. Park, A. K. R. Lytton Jean, B. Lee, S. Weigand, G. C. Schatz, C. A. Mirkin, *Nature* **2008**, *451*, 553 556.
[10] M. Meng, C. Ahlborn, M. Bauer, O. Plietzsch, S. A. Soomro, A. Singh, T. Muller, W. Wenzel, S. Bräse, C. Richert, *ChemBioChem* **2009**, *10*, 1335 1339.

[11] J. Zheng, J. J. Birktoft, Y. Chen, T. Wang, R. Sha, P. E. Constantinou, S. L. Ginnell, C. Mao, N. C. Seeman, *Nature* **2009**, *461*, 74 77.
[12] C. Richert, M. Meng, A. Singh, *Small* **2009**, *5*, 2782 2783.
[13] T. Hatano, T. Kato, *Tetrahedron* **2008**, *64*, 8368 8380.
[14] O. Plietzsch, C. I. Schilling, M. Tolev, M. Nieger, C. Richert, T. Muller, S. Bräse, *Org. Biomol. Chem.* **2009**, *7*, 4734 4743.
[15] For all DNA structures with embedded proteins, see for example: a) C. M. Erben, R. P. Goodman, A. J. Turberfield, *Angew. Chem.* **2006**, *118*, 7574 7577; *Angew. Chem. Int. Ed.* **2006**, *45*, 7414 7417; b) P. J. Paukstelis, *J. Am. Chem. Soc.* **2006**, *128*, 6794 6795.
[16] For exceptionally stable intramolecular duplexes, see for example: K. M. Herrlein, R. L. Letsinger, *Angew. Chem.* **1997**, *109*, 622 624; *Angew. Chem. Int. Ed. Engl.* **1997**, *36*, 599 601.